Microphase Transitions of Perforated Lamellae of Cyclic Diblock Copolymers under Steady Shear

Li-Yan You, Li-Jun Chen, Hu-Jun Qian, and Zhong-Yuan Lu*

State Key Laboratory of Theoretical and Computational Chemistry, Institute of Theoretical Chemistry, Jilin University, Changchun 130023, China

Received February 5, 2007; Revised Manuscript Received April 16, 2007

ABSTRACT: The dissipative particle dynamics simulation technique is used to study the microphase transitions of perforated lamellae of cyclic diblock copolymers under steady shear. The perforated lamellae are transformed to perfect lamellae, and the layer normal is aligned to the direction parallel to the gradient of the velocity under weak shear, whereas they undergo a phase transition to form perfect lamellae whose normal is aligned to the direction perpendicular to the gradient of the velocity due to strong shear. Subjected to the moderate shear, the perforated lamellae are transformed to hexagonally ordered cylinders. By examining the microphase morphologies in the shearing process, we find shear thinning in general, which is reflected by the reorientation of the lamellae, and shear-induced thickening when hexagonally ordered cylinders appear. The calculated shear viscosity basically decreases with increasing shear rate but shows a local maximum at the shear rate that induces hexagonally ordered cylinders.

1. Introduction

Recently, synthesizing the cyclic diblock copolymer and studying its physical properties are very active topics, because the material made of which possesses low viscosity due to the ring topology, which may facilitate the industrial processing. In general, four typical ordered morphologies upon microphase separation had been predicted and found in experiments, i.e., lamellae (LAM), hexagonally ordered cylinders (HEX), body-centered-cubic spheres (BCC), and bicontinuous gyroid (G), which are considered to be stable in equilibrium.[1−4] Except for these morphologies, various complex microphase structures had recently been observed in experiments, for example, the hexagonally perforated lamellae (HPL) and the hexagonally modulated lamellae.[4,5] Although these structures are metastable, they always appear in experiments by controlling the thermodynamic conditions. The HPL phase, which is residing between LAM and HEX in the phase diagram,[6−10] is of great interest because both of the transitions from HPL to HEX or from HPL to LAM are possible. Some experiments had revealed these kinds of transitions by tuning, for example, the experiment temperature.[11−14] The microphase structures of cyclic diblock copolymer were also extensively investigated in experiments.[15−20] The phase diagram of the cyclic diblock copolymer had been constructed, showing the regions that different microphases such as LAM, HEX, and HPL can be found.[21,22]

In experiments and during processing, the nonequilibrium conditions are commonly encountered. The shear flow can be regarded as an effective approach to break up the ordered microdomains and achieve another ordered microstructure. Shearing can not only lead into distinct microphases but also induce various orientations of the microphases, especially for the LAM architectures of diblock copolymers.[23−26] As for LAM, three orientations had been identified under shear: the parallel (i.e., the lamellar normal is parallel to the velocity gradient direction), the perpendicular (in which the lamellar normal is perpendicular to the velocity gradient direction), and the transverse orientation (that is, the lamellar normal is parallel to the velocity direction). In the recent decades, LAM under external perturbation had been comprehensively explored.[27−34]

Because of the novelty of the cyclic block copolymer and the importance of the knowledge on the microphase transition from perforated lamellae to other structures under shear, in this paper we show the study of the microphase transitions of HPL of cyclic block copolymers under steady shear using the dissipative particle dynamics (DPD) method. Indeed, computer simulations are convenient techniques in exploring the equilibrium structures and the dynamics of phase separation of polymeric materials. Some important simulation techniques include the time-dependent Ginzburg−Landau method (TDGL),[30,35] the dynamic density functional theory (DDFT),[36] the cell dynamic method,[37] the Monte Carlo method (MC),[38,39] the discontinuous molecular dynamics method (DMD),[40] the molecular dynamics method (MD),[41−43] and DPD.[44−46] On the basis of the simple models of free energy function, the DDFT technique was successful on modeling the coarse-grained polymer chains. TDGL method had been demonstrated to be another powerful tool for characterizing the mesoscopic dynamics of block copolymers. DMD was developed significantly to study long-time phenomena of polymers via discontinuous potential interactions. The MC method could simulate the microphase separation of a symmetric diblock copolymer and monitor changes in the energetic and the structural states of the system. In particular, the coarse-grained MD method had been generalized to study different systems, including investigating the nonequilibrium properties of these systems recently. DPD is established on the basic concept of the soft interacting particles which refer to a cluster of atoms or molecules. Especially, the DPD approach produces momentum conservation results and thus takes into account the rheological dynamics properties simultaneously. Liu et al. had studied the LAM reorientations of linear diblock copolymers due to shear flow using DPD.[47] To investigate the phase morphology of HPL of cyclic diblock copolymer, in this study, we have adopted a similar nonequilibrium DPD technique.

* To whom correspondence should be addressed. E-mail: luzhy@mail.jlu.edu.cn.

10.1021/ma0703103 CCC: $37.00
Published on Web 06/13/2007

2. Method and Simulation Details

In DPD, the pairwise interactive force acting on a particle i by the particle j contains three parts: the conservative force ($\mathbf{F}_{ij}^{C}$), the dissipative force ($\mathbf{F}_{ij}^{D}$), and the random force ($\mathbf{F}_{ij}^{R}$). The conservative force $\mathbf{F}_{ij}^{C}$, which is derived from a soft interaction potential within a certain cutoff radius r_c, is given by

$$\mathbf{F}_{ij}^{C} = \alpha_{ij}\omega^{C}(r_{ij})\mathbf{e}_{ij} \tag{1}$$

where $\mathbf{r}_{ij} = \mathbf{r}_i - \mathbf{r}_j$, $r_{ij} = |\mathbf{r}_{ij}|$, and $\mathbf{e}_{ij} = \mathbf{r}_{ij}/r_{ij}$. α_{ij} is the maximum repulsion between particle i and particle j. In order to ensure the conservative force soft and repulsive, the weight function $\omega^{C}(r_{ij})$ is chosen as $\omega^{C}(r_{ij}) = 1 - r_{ij}$ for $r_{ij} < 1$ and $\omega^{C}(r_{ij}) = 0$ for $r_{ij} \geq 1$. The number density in our simulations is 3. α_{ij} relates to the Flory−Huggins χ-parameter[45,48] via

$$\alpha_{ij} \approx \alpha_{ii} + 3.27\chi_{ij} \quad (\rho = 3) \tag{2}$$

In principle, ρ should be large enough to correctly describe the behavior of liquid.[45] We thus choose $\rho = 3$ for compromising between computation efficiency and the correctness of the model. The interaction parameter between the same type of particles α_{ii} equals 25, which is to correctly describe the compressibility of water, since it is a very representative quantity for a lot of liquids.[45]

The dissipative and the random forces are

$$\mathbf{F}_{ij}^{D} = -\zeta\omega^{D}(r_{ij})(\mathbf{v}_{ij}\cdot\mathbf{e}_{ij})\mathbf{e}_{ij} \tag{3}$$

$$\mathbf{F}_{ij}^{R} = \sigma\omega^{R}(r_{ij})\xi_{ij}\Delta t^{-1/2}\mathbf{e}_{ij} \tag{4}$$

where $\mathbf{v}_{ij} = \mathbf{v}_i - \mathbf{v}_j$. ζ is the dissipation strength which controls the heat dissipated in a time step, and σ is the noise strength with $\sigma = 3.67$. ξ_{ij} is a random number which has zero mean and unit variance. The weight functions $\omega^{D}(r_{ij})$ and $\omega^{R}(r_{ij})$ couple together to form a thermostat. Espanol and Warren[44] showed the relations between the two functions as

$$\omega^{D}(r) = [\omega^{R}(r)]^2$$
$$\sigma^2 = 2\zeta k_B T \tag{5}$$

We also choose the simple function form for $\omega^{D}(r_{ij})$ according to ref 45

$$\omega^{D}(r) = [\omega^{R}(r)]^2 = \begin{cases} (1-r)^2 & (r < 1) \\ 0 & (r \geq 1) \end{cases} \tag{6}$$

In the simulations, the radius of interaction, the particle mass, and the temperature are set as the unit, i.e., $r_c = m = kT = 1$.

When modeling polymers, the chains are constructed by connecting the adjacent particles via an extra harmonic spring[45]

$$\mathbf{F}_i^{S} = \sum_j C\mathbf{r}_{ij} \tag{7}$$

where the constant C is 4.0.

To impose steady shear, we use SLLOD equations of motion,[41] i.e.

$$\dot{\mathbf{r}}_i = \mathbf{p}_i/m + \mathbf{i}_x\dot{\gamma}r_{yi} \tag{8}$$

$$\dot{\mathbf{p}}_i = \mathbf{F}_i - \mathbf{i}_x\dot{\gamma}p_{yi} \tag{9}$$

where $\mathbf{r}_i$ and $\mathbf{p}_i$ are the position and the momentum of particle i, respectively. $\dot{\gamma}$ is the velocity profile with $\dot{\gamma} = \partial v_x/\partial r_y$. The planar shear flow profile is therefore

$$\mathbf{u} = \mathbf{i}_x\dot{\gamma}r_y \tag{10}$$

The flow direction is parallel to the X axis, the Y axis refers to the velocity gradient, and the Z axis represents the transverse direction. Meanwhile, we employ the Lees−Edwards periodic boundary condition (PBC) to maintain the linear velocity gradient.[41,49] The modified equations of motion are integrated via velocity Verlet algorithm with a time step of 0.03, which is chosen by compromising between the system stability and the computational efficiency.[45]

For the cyclic diblock copolymer characterized by A_mB_n ($N = m + n = 20$ in this study), the volume fraction f is $f = m/N$. By consulting the phase diagram of Qian et al.,[22] we select $f = 0.35$ and $\chi N = 110$, where the perforations of the layers are clear and hexagonally ordered. In general, the ordered equilibrium microphases of cyclic diblock copolymers are similar to those of the linear counterparts. Their phase diagrams are also very similar, which is attributed to the reduced chain length.[22,50] It should be noted that in equilibrium the HPL are not oriented to a certain direction such as parallel, perpendicular, and transverse as described above. In the simulations, the shear rate is carefully chosen to avoid microturbulence.[51] The simulation box size is $20 \times 20 \times 20$, which is large enough for our purpose as demonstrated by refs 22 and 47. Therefore, the cubic box accommodates 2400 polymer chains. Comprehensive simulations are conducted with the shear rate changing from 0.01 to 0.20 with the interval of 0.01. The simulation time ranges from 2×10^5 to 1×10^6 timesteps depending on the applied shear rate, which should ensure that the system reaches to the steady state and the time average can be decoupled from the phase transition process. In order to establish the comparison of the phase morphology, the same initial randomly oriented HPL phase is selected in all of the simulations.

3. Results and Discussion

3.1. Effects of Changing Shear Rate. The details of HPL phase transitions due to different shear rate are summarized in Table 1. The HPL phase is considered as a metastable phase residing on a saddle point in the free energy surface.[52] It can be transformed to LAM phase and HEX phase by varying shear rate, which was verified by some experiments.[5,12,14]

Table 1 can be roughly divided into three parts depending on the final microphase structures: LAM (from $\dot{\gamma} = 0.01$ to $\dot{\gamma} = 0.06$), HEX ($\dot{\gamma} = 0.07$ and 0.08), and LAM (from $\dot{\gamma} = 0.09$ to $\dot{\gamma} = 0.20$). When the relatively weak shear is applied, i.e., form 0.01 to 0.03, it takes about 1.5×10^5 timesteps to achieve the steady states, in which the lamellae do not align to the above-mentioned three standard orientations. The final morphologies are LAM with defects. Only small and irregular perforations appear locally during certain timesteps. They should not be considered as the re-formed HPL phase since in the course of shearing they exhibit the characteristics of LAM phase. With increasing shear rate, the dihedral angle between the LAM and the XY plane is increasing gradually as a result of the imposed shear. For example, the dihedral angle is 45° for $\dot{\gamma} = 0.01$, 71.5° for $\dot{\gamma} = 0.02$, and 75° for $\dot{\gamma} = 0.03$. The LAM phase tends to be parallel oriented with increasing $\dot{\gamma}$ and reaches the parallel alignment (i.e., the LAM normal parallel to the velocity gradient) when $\dot{\gamma} = 0.04$. Keeping on enhancing the shear, the parallel reorientation of the LAM phase disappears and the lamellae tilt again. The dihedral angle is 71.2° for $\dot{\gamma} = 0.05$ and 51° for

Table 1. Microphase Structures Depending on Shear Rate[a]

shear rate	timesteps	final morphology	parallel to axis?	orientation
0.01	1.5×10^5	LAM with defect	no	~45°
0.02	1.5×10^5	LAM with defect	no	~71.5°
0.03	1.5×10^5	LAM with defect	no	~75°
0.04	1×10^5	LAM	yes	parallel
0.05	1×10^5	LAM	no	~71.2°
0.06	1×10^5	LAM	no	~51°
0.07	1×10^5	HEX	yes	parallel to *X* axis
0.08	1×10^5	HEX	yes	parallel to *X* axis
0.09	1×10^5	LAM with defect	yes	perpendicular
0.10	1×10^5	LAM with defect	yes	perpendicular
0.11	1×10^5	LAM with defect	yes	perpendicular
0.12	1×10^5	LAM with defect	yes	perpendicular
0.13	1×10^5	LAM with defect	yes	perpendicular
0.14	1×10^5	LAM with defect	yes	perpendicular
0.15	5×10^4	LAM	yes	perpendicular
0.16	5×10^4	LAM	yes	perpendicular
0.17	5×10^4	LAM	yes	perpendicular
0.19	5×10^4	LAM	yes	perpendicular
0.20	5×10^4	LAM	yes	perpendicular

[a] Timesteps refer to the simulation times after which we can roughly obtain the final structures. The orientation represents the relationship between the lamellae normal and the velocity gradient for LAM phase, or the dihedral angle between the lamellae and the *XY* plane for the tilted lamellae, or the cylinder direction of the HEX phase.

$\dot{\gamma} = 0.06$. In these two cases, it needs less time to reach to the final structures, roughly after 1×10^5 timesteps. It seems that the LAM phase is changing from parallel to perpendicular orientation with increasing shear rate. It should be noted that from $\dot{\gamma} = 0.04$ to 0.06 the stable microphase structures are LAM without defects. The above results show that the shear flow can induce the phase transitions and speed up the rearrangement of microphase structures globally.[25,42]

Interestingly, HEX phases appear while $\dot{\gamma} = 0.07$ and $\dot{\gamma} = 0.08$, which are neither too strong nor too weak. However, in the case of $\dot{\gamma} = 0.07$, the HEX phase has slight defects, such as the rodlike connections between the two cylinders and the cylinders being not well hexagonally ordered. In the case of $\dot{\gamma} = 0.08$, the cylinders are stable and well hexagonally ordered. The HEX phase does not vanish while keeping on shearing. Moreover, the hexagonally ordered cylinders are all parallel to the *X* axis which represents the flow direction. This is in accordance with the results of experiments and theory,[11,12,14,52,53] which indicated the transition from HPL to HEX being possible.

When further increasing the shear rate, we find another HPL to LAM transition. Note that in these cases the LAM normal is perpendicular to the velocity gradient. Because of the stronger shear, it takes rather less time to achieve the perpendicular lamellae alignment. From $\dot{\gamma} = 0.09$ to $\dot{\gamma} = 0.14$, the LAM phase is always accompanied by some defects. But these defects will vanish gradually with increasing the shear rate. From $\dot{\gamma} = 0.15$ to $\dot{\gamma} = 0.20$, the perpendicular LAM phases, without defects, are found. It is clear that the strain of shear plays a significant role in controlling the lamellae reorientation during flow alignment of diblock copolymers.[25]

The phase transitions and reorientations also manifest the shear induced thinning and thickening. The initial randomly oriented HPL phase implies that the layer spacing cannot fit to the size of the box. By shearing, HPL phase is transformed to LAM phase, in which the layer spacing is apparently decreased so that LAM can take parallel or perpendicular orientations. It is attributed to the shear-induced thinning. In the phase transition from HPL to HEX, the layers are broken to form cylinders, whose diameter is larger than the width of the layer. This can be taken as the result of shear-induced thickening.

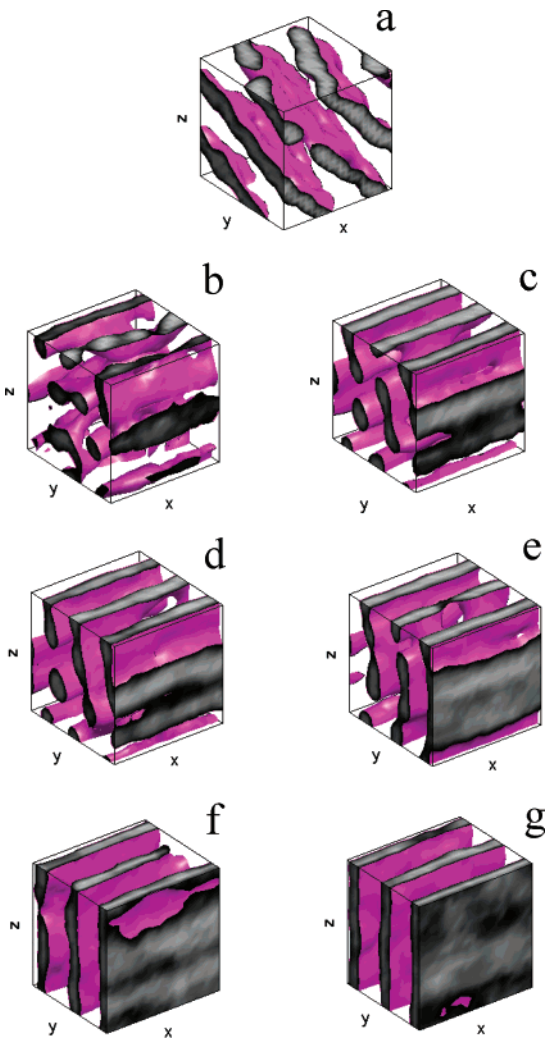

Figure 1. Simulation snapshots of the time evolution of HPL phase under weak shear, $\dot{\gamma} = 0.04$. The snapshots are taken every 1×10^4 timesteps.

3.2. Phase Morphology and Order Parameter. In our simulations, the same HPL initial configuration is used under various shear rate. Thus, the observed phase transitions do not depend on the initial configuration. There are two main time scales in the simulations: one is characterizing the phase transition during shearing, and the other is for ensemble (time) average. The first time scale is not known in advance but can be estimated within several "computer experiments". The second time scale for time average is always chosen large enough in the simulations. To track the morphology change of the HPL phase under shear, we show the isosurfaces of component A with density equal to 1.5 in Figure 1 for $\dot{\gamma} = 0.04$, Figure 2 for $\dot{\gamma} = 0.08$, and Figure 3 for $\dot{\gamma} = 0.20$. These shear rates represent the weak, the moderate, and the strong shear, corresponding to the distinct final microphase structures as parallel LAM, HEX, and perpendicular LAM, respectively. To compare the effect of box size, some extra simulations have been carried out by changing the box size to $25 \times 25 \times 25$. After much longer simulation time, similar results are found.

In Figure 1 (for $\dot{\gamma} = 0.04$), the snapshots are taken every 1×10^4 timesteps. Figure 1a shows the initial HPL phase, which is the same in all the simulations. It is shown in Figure 1b that the perforated layers are destroyed completely, and only irregular structures can be found. Subsequently, as shown in Figure 1c,d, the disordered structures start to connect with the adjacent ones along the flow direction and the vortex direction. There is no

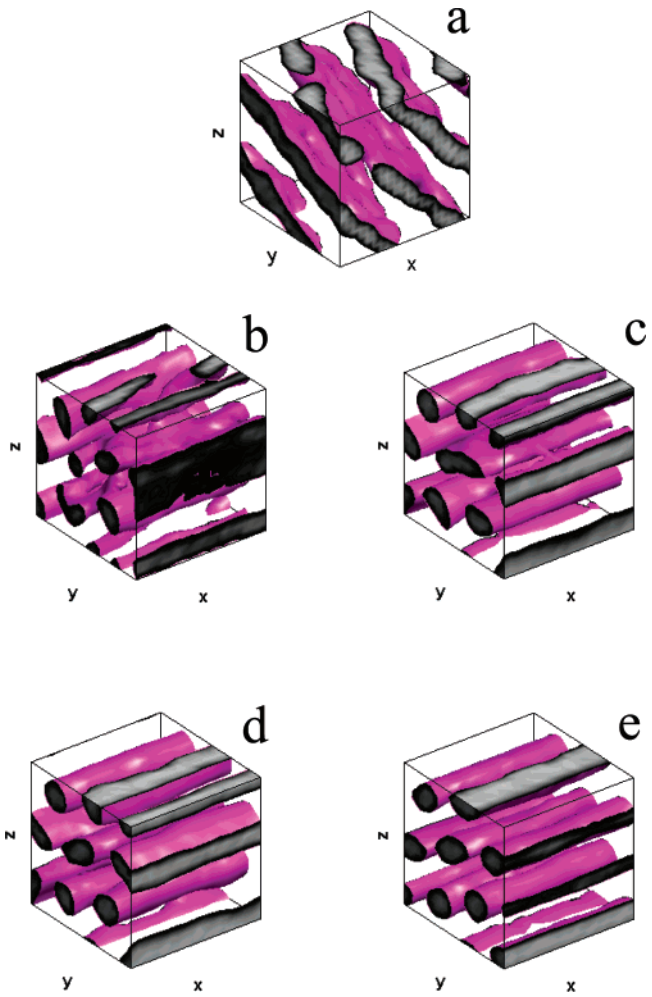

Figure 2. Simulation snapshots of the time evolution of HPL phase under moderate shear, $\dot{\gamma} = 0.08$. The snapshots are taken every 8×10^3 timesteps.

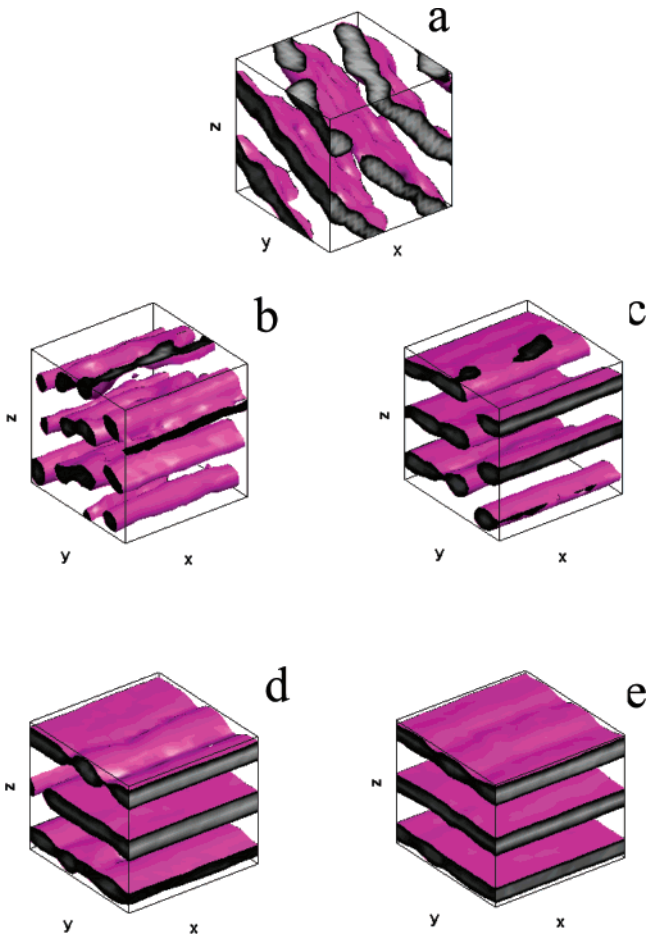

Figure 3. Simulation snapshots of the time evolution of HPL phase under strong shear, $\dot{\gamma} = 0.20$. The snapshots are taken every 5×10^3 timesteps.

big difference between parts c and d of Figure 1 except that the irregular lamellar structures in Figure 1d are less tilted compared to those in Figure 1c, which is attributed to the velocity gradient being along the *Y* axis. Later, the irregular lamellar structures join together, and the parallel lamellae with some defects are set up, as shown in Figure 1e. Over another 1×10^4 timesteps, as shown in Figure 1f, the lamellae are developed with fewer defects, and the normal is well aligned along the velocity gradient direction. Finally, Figure 1g obviously shows that the parallel aligned LAM appear, whose orientation is parallel to the velocity gradient. Figure 1 exhibits the slow evolution from HPL phase to the parallel LAM phase at comparatively small shear rate.

The snapshots in Figure 2 are taken every 8×10^3 timesteps. Figure 2a is the initial HPL phase. Figure 2b shows that the layers are broken and transformed to irregular structures. The structures are cylinder-like and are not disordered absolutely. Then, as shown in Figure 2c, the cylinder-like structures are merged with a lot of defects that some adjacent structures are still connected, and the hexagonal symmetry is absent. Figure 2d shows that the cylinders are aligned parallel to the flow direction and are more symmetric and uniform due to the influence of the shear. Figure 2e exhibits the long-range hexagonally ordered cylinders which are parallel to the flow direction under moderate shear rate $\dot{\gamma} = 0.08$. The HEX phase is stable at this shear rate because we have prolonged the simulation time over another 2×10^5 timesteps and found that the HEX phase still exists.

Figure 3 shows the phase transition from HPL to perpendicular LAM under strong shear with $\dot{\gamma} = 0.20$. The snapshots are taken at interval of 5×10^3 timesteps because the structures change quite fast. After 5×10^3 timesteps, the initial HPL phase (shown in Figure 3a) is totally broken, and cylinder-like structures appear under this strong shear, as shown in Figure 3b. These structures are random and interconnected with each other. After another 5×10^3 timesteps, some of the cylinder-like structures joint to form layers whose normal is perpendicular to the velocity gradient and others are still cylinder-like and parallel to the flow direction, as shown in Figure 3c. Subsequently, the mixture of the lamellae and the cylinders quickly transforms to the lamellae whose normal is perpendicular to the velocity gradient, as shown in Figure 3d. However, the lamellae are not flat. Figure 3e shows the emergence of the LAM phase whose orientation is perpendicular. The HPL phase thus undergoes a transition to LAM phase, whose orientation is perpendicular under strong shear, in contrast to the HPL−parallel LAM transition under weak shear. With another 2×10^5 timesteps simulation, the perpendicular LAM phase is still stable under shear.

The order parameter is defined by Saupe tensor:[54]

$$Q_{\alpha\beta} = \frac{3}{2}\left(\hat{r}_\alpha \hat{r}_\beta - \frac{1}{3}\delta_{\alpha\beta}\right) \tag{11}$$

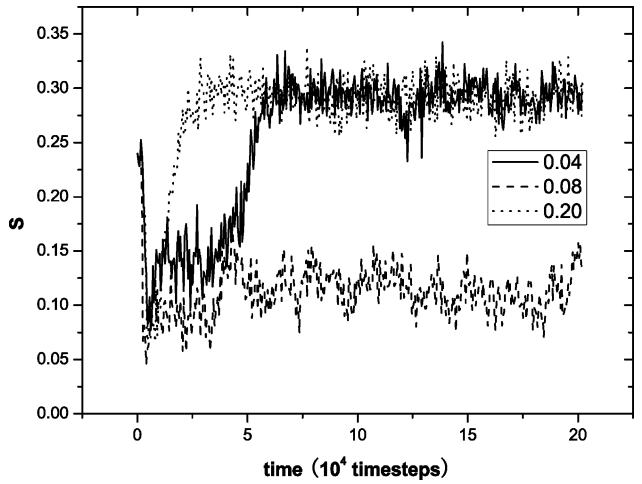

Figure 4. The order parameter (S) changes in the process of shearing on the HPL phase. Solid line represents $\dot{\gamma} = 0.04$, dashed line $\dot{\gamma} = 0.08$, and dotted line $\dot{\gamma} = 0.20$.

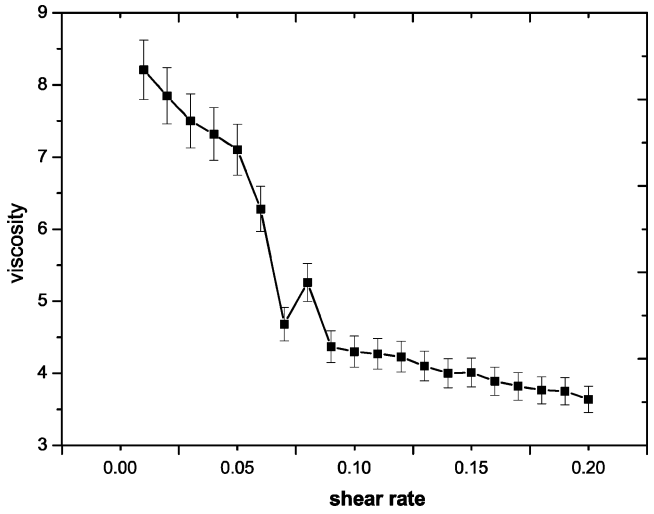

Figure 5. Shear viscosity vs shear rate.

where α and β are Cartesian indices, δ is the Kronecker symbol, and $\hat{\mathbf{r}}$ is a unit vector along the bond which connects the A block and the B block together. The largest eigenvalue of the volume average $Q_{\alpha\beta}$ is the order parameter S. S is zero for block copolymer in the completely disordered state and unity for block copolymer in the ordered alignment state.

We calculate the order parameters of the HPL phase under three typical shear rates, $\dot{\gamma} = 0.04$, $\dot{\gamma} = 0.08$, and $\dot{\gamma} = 0.20$, and show their changes with time in Figure 4. In the beginning, $S = 0.25$, which corresponds to the initial HPL phase. In the case of $\dot{\gamma} = 0.04$, the order parameter decreases gradually. It takes about 8×10^3 timesteps to reach its minimum, i.e., $S = 0.06$, corresponding to the random structures. Then S increases and fluctuates around 0.14 from 1×10^4 to 3.5×10^4 timesteps. It implies that the system is of some degree of ordering, which is consistent with the snapshots shown in Figure 1b,c. Subsequently, S increases gradually to reach the characteristic value for LAM, $S = 0.3$. This corresponds to the morphology as shown in Figure 1g. Under strong shear $\dot{\gamma} = 0.20$, S decreases in a very short time to its minimum of $S = 0.05$ and then S increases to 0.3 quite fast; the corresponding morphology in equilibrium is the LAM phase as shown in Figure 3e. The order parameters for $\dot{\gamma} = 0.04$ and 0.20 in final stable states are both around 0.30, which manifests the similarity of the LAM phase under different shear rates. The difference between these two cases is that it takes rather less time for the HPL−perpendicular LAM transition subjected to strong shear. It implies that shearing can speed up the phase transition. In the case of $\dot{\gamma} = 0.08$, S decreases quickly to reach the minimum, showing that the HPL phase is destroyed completely. Then S increases to a plateau value 0.10, which implies that the corresponding morphologies as shown in Figure 2b,c are not absolutely disordered. It takes about 4×10^4 timesteps for S to increase to a value of 0.13, which corresponds to the HEX phase as shown in Figure 2e. The order parameters in these three cases show the dynamics during transition under shear. S always rapidly goes through a minimum which corresponds to the disordered structure and increases gradually to the characteristic values for the target stable phases. Thus, shear rate plays a crucial role in phase behavior of cyclic diblock copolymer which is in agreement with the results of ref 25.

3.3. Shear Viscosity. Shear viscosity directly relates to the pressure tensor, which is measured by[41,45]

$$P_{\alpha\beta} = \frac{1}{V}\langle \sum_i m_i v_{i,\alpha} v_{i,\beta} \rangle + \frac{1}{V}\langle \sum_i \sum_{j>i} F^{C}_{ij,\alpha} r_{ij,\beta} \rangle \qquad (12)$$

where V is the volume of the simulation box. It is critical to verify that the three diagonal components of the pressure tensor P_{xx}, P_{yy}, and P_{zz} are equal to each other in equilibrium. In our simulations, the box size in the Y direction can be adjusted to fit the requirement of the pressure tensor. However, we find no apparent difference of phase behavior by adjusting the box size. Shear viscosity in association with the only nonvanishing off-diagonal component $P_{xy} = -P_{yx}$ is given by

$$\eta = -\frac{P_{xy}}{\dot{\gamma}} \qquad (13)$$

where η is the non-Newtonian shear viscosity.

Both Koppi et al.[23] in experiment and Guo[43] by MD simulation had argued that the shear viscosity relates to the orientation of the LAM phase, i.e., $\eta_{\text{perpendicular}} < \eta_{\text{parallel}}$. The calculated shear viscosity as a function of shear rate is shown in Figure 5, from which three regions corresponding to different phases and orientations can be identified. The first region corresponds to the small shear rates with $\dot{\gamma} < 0.05$, where the shear viscosity is large. In this region the shear viscosity decreases gradually with increasing shear rate until the parallel LAM phase is formed at $\dot{\gamma} = 0.04$. After that, the shear viscosity decreases dramatically until $\dot{\gamma} = 0.07$ and shows a local maximum at $\dot{\gamma} = 0.08$. In this region the LAM phase (not parallel to any particular direction) is tilting and transforming to the HEX phase. The shear viscosity decreases smoothly with increasing shear rate in the third region, where the perpendicular LAM phase is found. In our cases, $\eta_{\text{perpendicular}}$ is also smaller than η_{parallel}, which is in agreement with the results of refs 23 and 43. In general, the shear viscosity decreases with increasing shear rate, which corresponds to the shear thinning, whereas the local maximum of η at $\dot{\gamma} = 0.08$ corresponds to the shear-induced thickening.

4. Conclusions

In this study, we perform DPD simulations to investigate the microphase transitions of the HPL phase of cyclic diblock copolymers under steady shear flow. It is a challenge to comprehensively investigate the microphase transitions when the HPL phase subjected to the steady shear, which is rarely studied before. In this study we have not tried to construct the whole phase diagram for the cyclic diblock copolymer under

shear. Actually, the phase diagram is shear rate dependent. Instead, we focus on the detailed transition behavior of HPL phase under different shear rates. Both HPL−LAM and HPL−HEX transitions are identified. We choose a series of shear rates in order to compare the changes of the final stable structures. The process of phase transition and the properties of the cyclic diblock copolymer are quite sensitive to the strength of shear rate. The application of shear can be roughly classified by three kinds, not only according to the strength but also according to the final microstructures induced by the steady shear. We have monitored the evolution of phase transitions of the system by taking snapshots. For small shear rate, the HPL phase transforms to parallel LAM phase; for high shear rate, the HPL phase transforms to perpendicular LAM phase. It is interesting that the HPL phase changes to form HEX phase at moderate shear rate. Enhancing shear rate can speed up the phase transition. On the other hand, we track the instantaneous structural evolution via the order parameter as a function of shear rate and time. We find that the three phase transition procedures all undergo the disordered state, where the minimum values of order parameter for the three typical shear rates are nearly the same, and these disordered phases will achieve the ordered orientational structures within different timesteps. By examining the microphase morphologies in the shearing process, we find shear thinning in general, which is reflected by the reorientation of the lamellae, and shear-induced thickening when hexagonally ordered cylinders appear. The calculated shear viscosity basically deceases with increasing shear rate but shows a local maximum at the shear rate that induces hexagonally ordered cylinders. It is worth mentioning that the shear viscosity relates to the final orientation of LAM structure. The shear viscosity of the perpendicular LAM is obviously quite smaller than that of the parallel LAM phase.

Acknowledgment. This work is supported by the National Science Foundation of China (20490220, 20404005) and JLSTP (20050562).

References and Notes

(1) Leibler, L. *Macromolecules* **1980**, *13*, 1602.
(2) Bates, F. S.; Fredrickson, G. H. *Annu. Rev. Phys. Chem.* **1990**, *41*, 525.
(3) Fredrickson, G. H.; Bates, F. S. *Annu. Rev. Mater. Sci.* **1996**, *26*, 501.
(4) Hamley, I. W. *The Physics of Block Copolymer*; Oxford University Press: New York, 1998.
(5) Hajduk, D. A.; Harper, P. E.; Gruner, S. M.; Honeker, C. C.; Thomas, E. L.; Fetters, L. J. *Macromolecules* **1994**, *27*, 4063.
(6) Fredrickson, G. H. *Macromolecules* **1991**, *24*, 3456.
(7) Olvera de la Cruz, M.; Mayers, A. M.; Swift, B. W. *Macromolecules* **1992**, *25*, 944.
(8) Hamley, I. W.; Bates, F. S. *J. Chem. Phys.* **1994**, *100*, 6813.
(9) Khandpur, A. K.; Koopi, K. A.; Bates, F. S. *Macromolecules* **1995**, *25*, 8796.
(10) Thomas, E. L.; Anderson, D. M.; Henkee, C. S.; Hoffman, D. *Nature (London)* **1988**, *334*, 598.
(11) Almdal, K.; Koppi, K.; Bates, F. S.; Mortensen, K. *Macromolecules* **1992**, *25*, 1743.
(12) Mani, S.; Weiss, R. A.; Cantino, M. E.; Khairallah, L. H.; Hahn, S. F.; Williams, C. E. *Eur. Polym. J.* **2000**, *36*, 215.
(13) Loo, Y. L.; Register, R. A.; Adamson, D. H.; Ryan, A. J. *Macromolecules* **2005**, *38*, 4947.
(14) Lai, C. J.; Loo, Y. L.; Register, R. A. *Macromolecules* **2005**, *38*, 7098.
(15) Benmouna, M.; Borsali, R.; Benot, H. *J. Phys. II* **1993**, *3*, 1401.
(16) Borsali, R.; Benmouna, M. *Europhys. Lett.* **1993**, *23*, 263.
(17) Borsali, R.; Benmouna, M.; Benoît, H. *Physica A* **1993**, *201*, 129.
(18) Benmouna, M.; Borsali, R. *J. Polym. Sci., Part B: Polym. Phys.* **1994**, *32*, 981.
(19) Borsali, R.; Benmouna, M. *Makromol. Chem. Symp.* **1994**, *79*, 153.
(20) Borsali, R.; Lecommandoux, S.; Pecora, R.; Benot, H. *Macromolecules* **2001**, *34*, 4229.
(21) Morozov, A. N.; Fraaije, J. G. E. M. *Macromolecules* **2001**, *34*, 1526.
(22) Qian, H. J.; Lu, Z. Y.; Chen, L. J.; Li, Z. S.; Sun, C. C. *Macromolecules* **2005**, *38*, 1395.
(23) Koopi, K. A.; Tirrell, M.; Bates, F. S.; Almdal, K.; Colby, R. H. *J. Phys. II* **1992**, *2*, 1941.
(24) Kannan, R. M.; Bates, F. S. *Macromolecules* **1994**, *27*, 1177.
(25) Gupta, V. K.; Krishnamoorti, R.; Kornfield, J. A.; Smith, S. D. *Macromolecules* **1996**, *29*, 1359.
(26) Chen, Z. R.; Kornfield, J. A.; Smith, S. D.; Grothaus, J. T.; Satkowski, M. M. *Science* **1997**, *277*, 1248.
(27) Polis, D. L.; Winey, K. I. *Macromolecules* **1998**, *31*, 3617.
(28) Pinheriro, B. S.; Hajduk, D. A.; Gruner, S. M.; Winey, K. I. *Macromolecules* **1996**, *29*, 1482.
(29) Maring, D.; Wiesner, U. *Macromolecules* **1997**, *30*, 660.
(30) Ohta, T.; Kawasaki, K. *Macromolecules* **1986**, *19*, 2621.
(31) Ren, S. R.; Hamley, I. W. *Macromolecules* **2001**, *34*, 116.
(32) Zryd, J. L.; Burghardt, W. R. *Macromolecules* **1998**, *31*, 3656.
(33) Cates, M. E.; Milner, S. T. *Phys. Rev. Lett.* **1989**, *62*, 1856.
(34) Wang, H.; Kesani, P. K.; Balsara, N. P.; Hammouda, B. *Macromolecules* **1997**, *30*, 982.
(35) Luo, K. F.; Yang, Y. L. *Macromolecules* **2002**, *35*, 3722.
(36) Fraaije, J. G. E. M. *J. Chem. Phys.* **1993**, *99*, 9202.
(37) Oono, Y.; Puri, S. *Phys. Rev. A* **1988**, *38*, 434.
(38) Fried, H.; Binder, K. *J. Chem. Phys.* **1991**, *94*, 8349.
(39) Pakula, T.; Karatasos, K.; Anastasiadis, S. H.; Fytas, G. *Macromolecules* **1997**, *30*, 8463.
(40) Schultz, A. J.; Hall, C. K.; Genzer, J. *J. Chem. Phys.* **2002**, *117*, 10329.
(41) Allen, M. P.; Tildesley, D. J. *Computer Simulation of Liquids*; Clarendon Press: Oxford, 1987.
(42) Guo, H. X.; Kremer, K. *J. Chem. Phys.* **2003**, *119*, 9308.
(43) Guo, H. X. *J. Chem. Phys.* **2006**, *124*, 054902.
(44) Espanol, P.; Warren, P. B. *Europhys. Lett.* **1995**, *30*, 191.
(45) Groot, R. D.; Warren, P. B. *J. Chem. Phys.* **1997**, *107*, 4423.
(46) Groot, R. D.; Madden, T. J. *J. Chem. Phys.* **1998**, *108*, 8713.
(47) Liu, W.; Qian, H. J.; Lu, Z. Y.; Li, Z. S.; Sun, C. C. *Phys. Rev. E* **2006**, *74*, 021802.
(48) Groot, R. D.; Rabone, K. L. *Biophys. J.* **2001**, *81*, 725.
(49) Lees, A. W.; Edwards, S. F. *J. Phys.* **1972**, *C5*, 1921.
(50) Marko, J. F. *Macromolecules* **1993**, *26*, 1442.
(51) Rychkov, I. *Macromol. Theory Simul.* **2005**, *14*, 207.
(52) Qi, S. Y.; Wang, Z. G. *Phys. Rev. E* **1997**, *55*, 1982.
(53) Luo, K. F.; Yang, Y. L. *Polymer* **2004**, *45*, 6745.
(54) de Gennes, P. G.; Prost, J. *The Physics of Liquid Crystals*; Clarendon Press: Oxford, 1993.

MA0703103